Hindawi Publishing Corporation
Journal of Nanomaterials
Volume 2016, Article ID 3623547, 12 pages
http://dx.doi.org/10.1155/2016/3623547

Research Article

Electrodeposition-Based Fabrication and Characteristics of Tungsten Trioxide Thin Film

Li Lin,[1] Chin-Pao Cheng,[2] and Tun-Ping Teng[1]

[1]*Department of Industrial Education, National Taiwan Normal University, No. 162, Section 1, He-ping E. Road, Da-an District, Taipei City 10610, Taiwan*
[2]*Department of Mechatronic Engineering, National Taiwan Normal University, No. 162, Section 1, He-ping E. Road, Da-an District, Taipei City 10610, Taiwan*

Correspondence should be addressed to Tun-Ping Teng; tube5711@ntnu.edu.tw

Received 28 November 2015; Revised 18 February 2016; Accepted 29 March 2016

Academic Editor: Zainovia Lockman

In this study, tungsten trioxide (WO_3) thin films were electrodeposited on indium tin oxide (ITO) glass to form WO_3-coated glass. The electrodeposition (ED) time (t_{ED}) and ED current (I_{ED}) were varied to control the film thickness and morphology. Furthermore, the crystallization of the thin films was controlled by annealing them at 250°C, 500°C, and 700°C. The results showed that the thickness of the WO_3 thin films increased with t_{ED} and I_{ED}. The as-deposited thin films and those annealed at 250°C were amorphous, whereas the WO_3 thin films annealed at 500 and 700°C were in the anorthic phase. Moreover, the amorphous WO_3-coated glass exhibited high transmittance in visible light and low transmittance in near-infrared light, whereas the anorthic WO_3-coated glass had high transmittance in near-infrared light. An empirical formula for determining the thickness of WO_3 thin films was derived through multiple regressions of the ED process parameters.

1. Introduction

Tungsten trioxide (WO_3) is a transition metal oxide and an n-type semiconductor. Different forms of crystalline have unique optical, electrical, and magnetic properties and are widely used in various fields. WO_3 has electrochromic properties and is widely used in reversible electrochromic elements, smart windows, and mirrors [1–7]. It also shows high catalytic performance in degrading contaminants, often in combination with TiO_2, Pt, Ag, Na^+, and other materials [8–11]. Furthermore, WO_3 is used in gas sensors because of its sensitivity to various gases such as CO, ethanol gas, NH_3, NO_x, ozone, and toluene gas [12–16]. In addition to the aforementioned applications, WO_3 can be used in lithium-ion battery electrodes [17–20] and for lubricating mechanical components [21–23] to improve their operating performance. Therefore, WO_3 has high potential for use in developing multifunctional materials. Because of their characteristics, WO_3 materials can be employed to modify traditional materials and endow them with specific characteristics to improve their performance.

WO_3 thin films are typically fabricated using such methods as chemical vapor deposition [12, 24], sputtering [5, 6, 16], screen printing [12, 14], and electrodeposition (ED) [1–3, 25, 26]. ED involves a simple setup, is inexpensive, does not require special atmospheric conditions, and can easily form thin films on irregularly shaped substrates. WO_3 thin films can be fabricated by using peroxotungstic acid in the ED process, and their thickness and morphology can be controlled by varying the ED voltage (V_{ED}), current (I_{ED}), and time (t_{ED}). Generally, ED is commonly used along with a three-electrode electrochemical cell in preparing a WO_3 thin film [1–3, 25–27].

In this study, ED using a two-electrode method was employed to fabricate a WO_3 thin film on an indium tin oxide (ITO) glass substrate. The ED of the two-electrode method has advantages of lower equipment cost and higher deposition rate than the three-electrode electrochemical cell.

By adjustment of the t_{ED} and I_{ED}, the structure, thickness, and morphology of the thin films were controlled. Furthermore, the crystallization of the thin films was controlled by annealing them at various temperatures (T_a). Finally, an ultraviolet-visible-near-infrared (UV-VIS-NIR) spectrometer was used to determine the spectral characteristics of the WO_3-coated glass.

2. Preparation of WO_3 Thin Films

The primary materials used for preparing peroxotungstic acid were tungsten metal powder (particle size: 12 μm; purity: 99.9%; Acros, Belgium) and a low concentration (34.5%–36.5%) of hydrogen peroxide (H_2O_2, Sigma-Aldrich, Germany). Dissolving 3.0 g of tungsten metal powder in 30 mL of H_2O_2 yielded a colorless peroxotungstic acid solution. The exothermic reaction was conducted by cooling the acid solution in an isothermal unit (P-10, YSC, Taiwan) between 5°C and 10°C. The reaction formula for peroxotungstic acid preparation is as follows [25, 27]:

$$2W + 10H_2O_2 \longrightarrow {W_2O_{11}}^{2-} + 2H^+ + 9H_2O \quad (1)$$

When the exothermic reaction was completed, the solution was filtered using filter paper (pore size, 10-μm) to remove the unreacted tungsten powder. The obtained clear solution was combined with 30 mL of 99.7% glacial acetic acid (CH_3COOH, Showa, Japan), and the resulting solution was refluxed at 55°C for 12 h to decompose excess H_2O_2 and acetylate the peroxotungstic acid. Refluxing the peroxotungstic acid strengthened the adhesion between the thin film and the substrate [1]. Finally, the refluxed peroxotungstic acid was mixed with 60 mL of anhydrous absolute ethanol to produce a pale yellow coating solution for the ED.

Figure 1 shows the experimental setup used in this study. To adjust the electrode distance (20 mm), a platinum plate and ITO glass substrate (7 Ω/cm^2, 1737, Corning, USA) were fixed to a polypropylene holder as the positive and negative electrodes. The holder was placed in a glass tank containing a thermoelectric module and temperature controller. Prior to ED, the ITO glass was cleaned to remove contaminants and improve the adhesion between the ITO glass surface and WO_3 thin film. The ITO glass was cleaned in acetone for 20 min in an ultrasonic bath (5510R-DTH, Branson, USA), rinsed with deionized water, dried in nitrogen (N_2, 99.995%), and heated to 60°C for 15 min on a hot plate (PC-420D, Corning, USA).

The platinum plate and ITO glass electrodes measured 30 mm × 20 mm × 0.8 mm (L × W × Thickness) and 20 mm × 20 mm × 0.6 mm (L × W × Thickness), respectively; the length of the electrode immersed in the coating solution was 18 mm. Therefore, the effective area of platinum plate and ITO glass electrodes for ED was approximately 7.5 and 3.6 cm^2, respectively. Through ED, a WO_3 thin film was formed on the ITO glass (negative electrode). Because the coating solution temperature affects the electrochemical reaction, the thermoelectric module was necessary to maintain the coating solution temperature at 15°C to preserve the stability and reproducibility of the WO_3 thin-film fabrication process.

This study used ED along with two-electrode equipment (programmable DC power supply) and a constant I_{ED} process for preparing a WO_3 thin film on ITO glass. This approach is advantageous because it involves low equipment costs and a simple process and achieves a relatively stable coating rate. The reaction formula of ED with peroxotungstic acid for the WO_3 thin-film preparation is as follows [25, 27]:

$${W_2O_{11}}^{2-} + 2H^+ \longrightarrow 2WO_3 + 2O_2 + H_2O \quad (2)$$

In the ED process, a programmable DC power supply (PSS-3203, GW Instek, Taiwan) was used to maintain a constant I_{ED} (3, 5, 7, and 9 mA) for various t_{ED} (30, 40, 50, and 60 s). The current density for 3, 5, 7, and 9 mA of I_{ED} on the ITO electrode was approximately 0.83, 1.39, 1.94, and 2.50 mA/cm^2, respectively. After the thin films were fabricated, the WO_3-coated glass was cleaned by rinsing it with deionized water, drying it in N_2, and heating it to 60°C for 10 min on a hot plate. WO_3-coated glass samples were selected on the basis of preferred ED process parameters, which were determined according to the morphology of the WO_3 thin films; the morphology was observed using visually and optical microscope. The selected WO_3-coated glass samples were annealed at 250°C, 500°C, and 700°C for one hour. The annealing temperatures of 250°C, 500°C, and 700°C for WO_3-coated glass mainly referred to the literature [1–3, 28, 29]. In general, in the annealing temperature of 350–550°C, the monoclinic WO_3 phase was naturally formed, while the formation of triclinic (anorthic) WO_3 phase was induced in the annealing temperature ranging from 550°C to 750°C. Above 750°C, the WO_3 phase can be changed to orthorhombic phase [6]. The annealed samples were then cleaned according to the aforementioned procedure. The ED process parameters are listed in Table 1. For each process parameter, three samples were prepared for testing to ensure the reproducibility and reliability of the relevant experiments.

3. Characterization

The surface morphologies of the WO_3 thin films were analyzed using a high-resolution field-emission scanning electron microscope (FESEM, S-4800, Hitachi, Japan). Crystallization was analyzed using a multifunction high-power X-ray diffractometer (XRD, D8 Discover SSS, Bruker, the Netherlands) with Cu Kα radiation, and all peaks measured by XRD were assigned by comparing them with those in the data of the International Centre for Diffraction Data [29].

The thickness of the WO_3 thin films was determined by the height of film cross section, which was measured using the FESEM. The high magnification of the film cross section caused the observation range to be very small, which limited the representative of the film thickness. Therefore, the WO_3 film thickness was also measured with a thin-film analyzer (F10-RT, Filmetric, USA); the measurement principle in this instrument is based on light interference in thin films. The crystallization will affect the refractive index and surface roughness of WO_3 thin film, thereby affecting the accuracy of the thickness of a WO_3 thin film measured by a thin-film analyzer. Therefore, the relevant setting parameters of

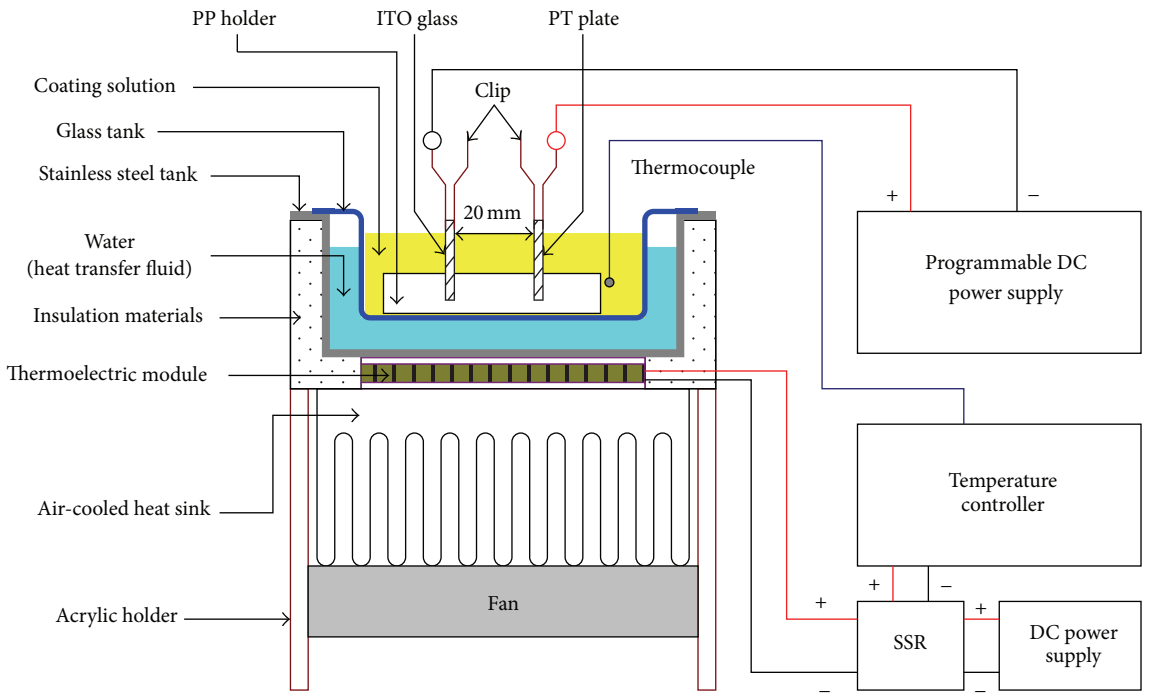

Figure 1: Experimental setup for ED.

Table 1: Process parameters of ED for the WO_3 thin films.

Number	I_{ED} (mA)	t_{ED} (sec.)	T_a (°C)*
1	3	30	As-deposited
2		40	250
3		50	500
4		60	700
5	5	30	As-deposited
6		40	250
7		50	500
8		60	700
9	7	30	As-deposited
10		40	250
11		50	500
12		60	700
13	9	30	As-deposited
14		40	250
15		50	500
16		60	700

*Only selected WO_3 coated glass to be annealed.

the thin-film analyzer were corrected according to the test results of cross sections of the WO_3 thin film measured by a FESEM to reduce the effects of refractive index and surface and roughness of the WO_3 thin film on thickness measurement. To minimize measurement deviations, each fabricated process parameter (for three samples) for the film thickness involved three measurements (one measurement of the cross section by using the FESEM and two measurements of the thickness with the thin-film analyzer; each process parameter consists of a total of nine measured data). The five most concentrated measurements were then averaged, and this value was considered the experimental value of the samples.

The optical characteristics of WO_3-coated glass for various process parameters were measured using a UV-VIS-NIR spectrometer (V-670, Jasco, Japan) with an integrating sphere (ISN-723, Jasco, Japan) to measure transmittance and reflectivity changes at wavelengths between 300 and 2400 nm at room temperature.

4. Results and Discussions

Figure 2 displays a photograph of a WO_3-coated glass sample, along with various process parameters. The lower edge of the sample shows discoloration or stripping when the I_{ED} is higher than 5 mA. Therefore, process parameters corresponding to the I_{ED} values of 3 and 5 mA (range of the red dotted line) were considered in the subsequent experiments.

Figure 3 shows FESEM images of a WO_3 thin film, along with various process parameters. An increase in I_{ED} and t_{ED} increased the surface roughness of the as-deposited WO_3 thin film (Figure 3(a)). This observation was attributed to the ED rate increasing with I_{ED}, which caused the surface of the WO_3 thin film to become increasingly uneven. In addition, the circuit impedance increased with the deposited film thickness, resulting in an unstable ED rate at long t_{ED}. Generally, a constant current leads to a relatively stable ED rate. However, the circuit impedance at each point on the thin-film surface during ED is affected by the uniformity of the film thickness and can cause the ED rate to fluctuate, which further affects

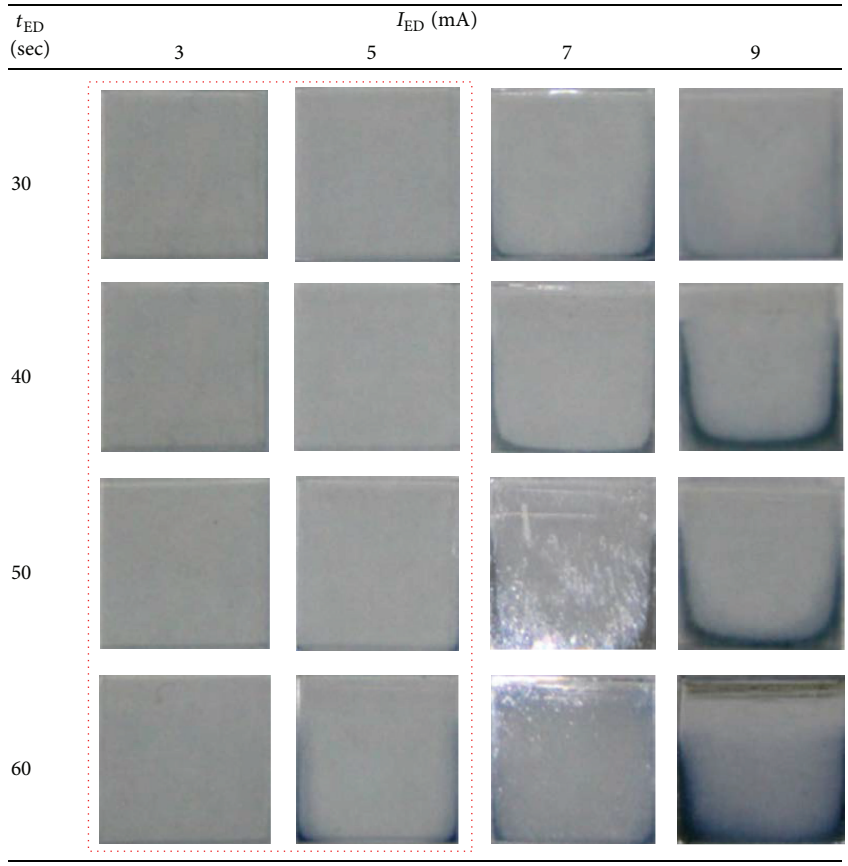

Figure 2: Photograph of the WO_3-coated glass, along with various process parameters.

the surface roughness and uniformity of the deposited film. The relationship between the crystallization of the WO_3 thin film and T_a can be analyzed as follows. In Figure 3(b), at T_a = 250°C, the surface morphologies of the WO_3 thin films become compact, but no notable crystallization occurs. When the T_a were 500 and 700°C, crystallization and crystal growth were evident (Figures 3(c) and 3(d)).

The diffraction patterns in Figures 4 and 5 show only the effect of the crystallization at various T_a at t_{ED} = 60 s. The reason for selecting this t_{ED} is that changes in the crystallization are easier to measure accurately in thicker films, and there is less interference in the diffraction signals from the substrate (ITO glass). The WO_3 thin films grown at the as-deposited temperature and at T_a = 250°C did not show any crystallinity and were amorphous [27]. However, after annealing at 500 and 700°C, the anorthic (triclinic) phase (PDF numbers: 20-1323) [2, 3] appeared; this was seen in the diffraction pattern, and the XRD and FESEM analyses yielded the same result at this T_a. The intensity of the (2 0 0) peak increased with T_a and I_{ED}, mainly because a higher I_{ED} leads to a thicker WO_3 thin film at a given t_{ED}, and a high T_a results in the formation of an almost perfectly crystalline WO_3 thin film.

Figure 6 is a cross-sectional FESEM image of the WO_3-coated glass annealed at 250, 500, and 700°C. The cross section shows a three-layer structure comprising WO_3, ITO, and glass. Defects formed in the glass substrate at T_a = 700°C may result from some ingredients or impurities melted in the glass substrate. Defects could affect the experimental determination of the optical characteristics and film thickness, which were measured using a spectrometer and thin-film analyzer. Therefore, the WO_3-coated glass annealed at 700°C was omitted from the subsequent measurements of the optical characteristics and film thickness.

Figure 7 shows the variation of WO_3 film thickness with various process parameters. The WO_3 film thickness increases with t_{ED} and I_{ED}. However, the T_a substantially affected the WO_3 film thickness. The thicknesses of the as-deposited WO_3 thin films at I_{ED} values of 3 and 5 mA were 132.8 and 216.1 nm at t_{ED} = 60 s, respectively, and the ED rate was considerably high. The moisture of the WO_3 thin film was removed, and the film became compact at T_a = 250°C; thereby, its average film thickness decreased. As the annealing temperature was raised to 500°C, some parts of the crystals grew larger to make the WO_3 thin film become thicker at these parts but thinner at other parts, exhibiting an uneven morphology of the thin-film surface (Figure 3(c)) and increased average film thickness of WO_3. In addition, increase in the film thickness of WO_3 may result from change of the structure in the process of crystalline phase transition for WO_3 thin film. The multiple regressions for deriving an empirical formula for the film thickness showed that the t_{ED}

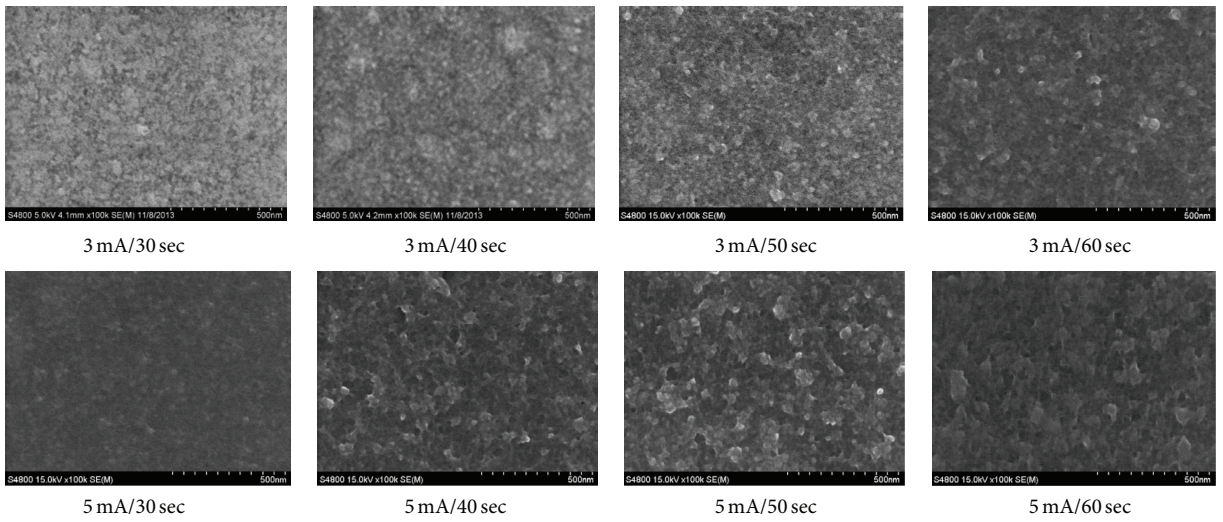

3 mA/30 sec 3 mA/40 sec 3 mA/50 sec 3 mA/60 sec

5 mA/30 sec 5 mA/40 sec 5 mA/50 sec 5 mA/60 sec

(a)

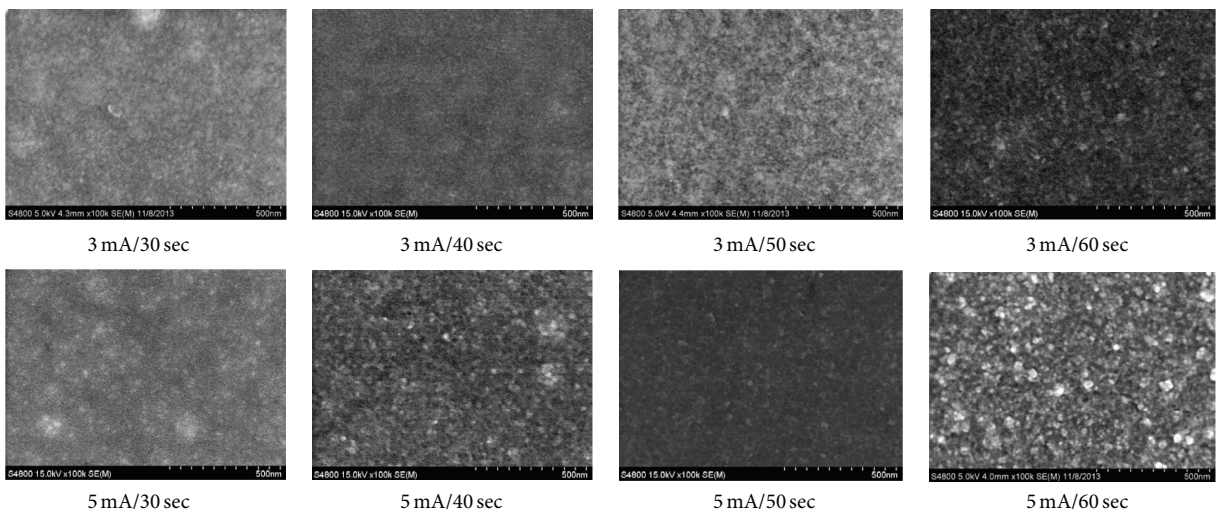

3 mA/30 sec 3 mA/40 sec 3 mA/50 sec 3 mA/60 sec

5 mA/30 sec 5 mA/40 sec 5 mA/50 sec 5 mA/60 sec

(b)

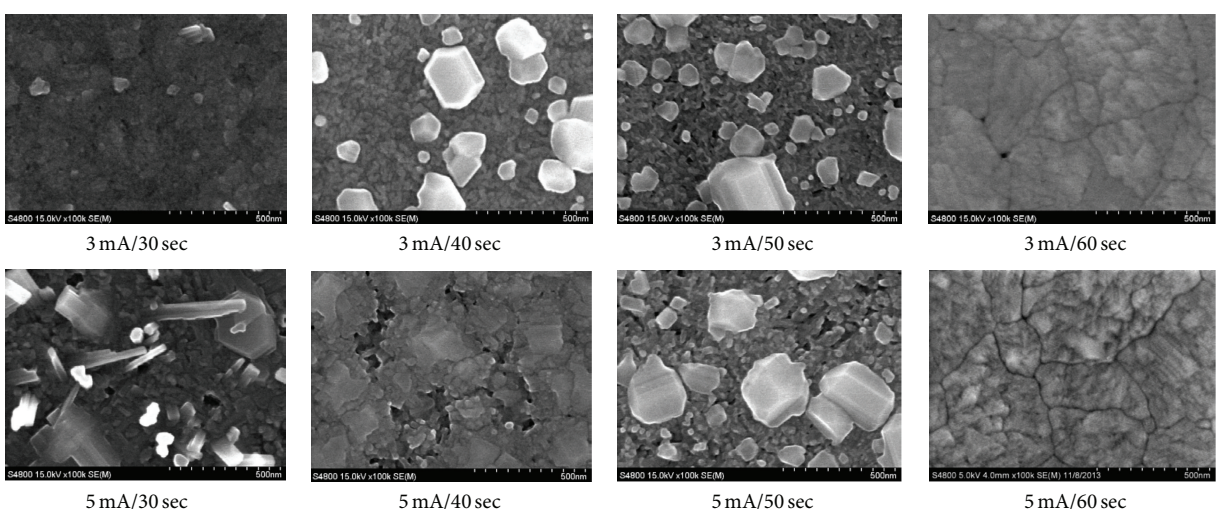

3 mA/30 sec 3 mA/40 sec 3 mA/50 sec 3 mA/60 sec

5 mA/30 sec 5 mA/40 sec 5 mA/50 sec 5 mA/60 sec

(c)

Figure 3: Continued.

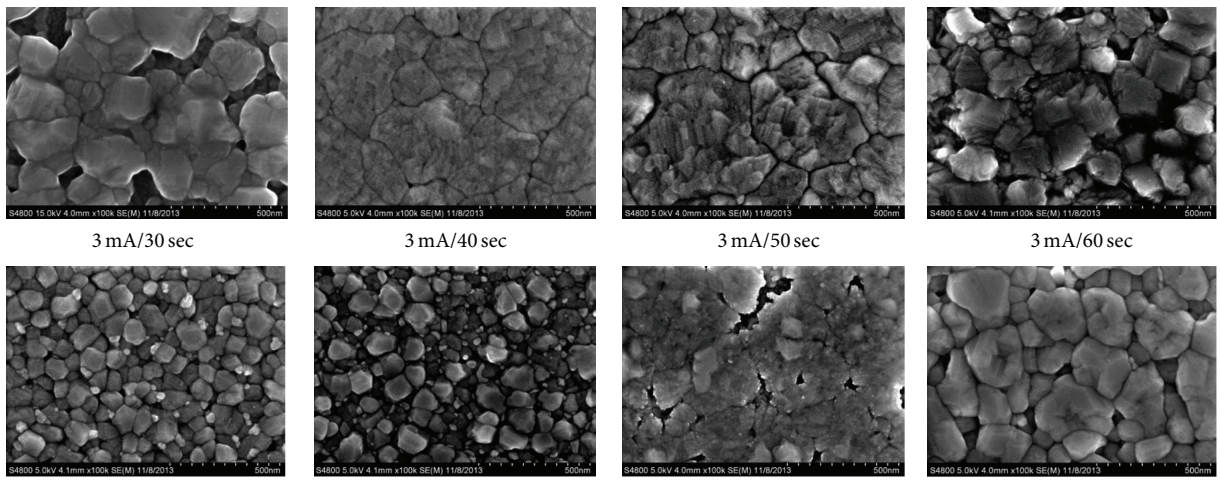

FIGURE 3: FESEM images of WO_3 thin films, along with various process parameters: (a) as-deposited, (b) T_a = 250°C, (c) T_a = 500°C, and (d) T_a = 700°C.

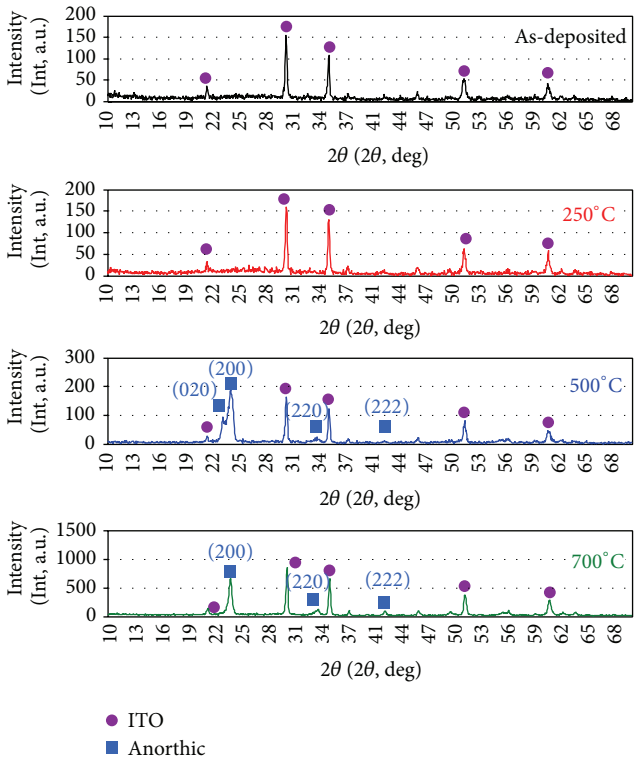

FIGURE 4: XRD pattern for the WO_3-coated glass annealed at various T_a and an I_{ED} of 3 mA.

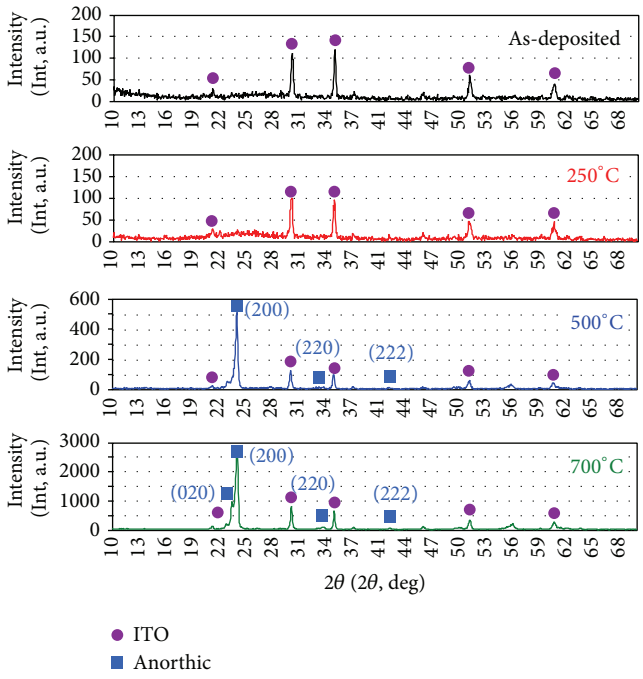

FIGURE 5: XRD pattern for the WO_3-coated glass annealed at various T_a and an I_{ED} of 5 mA.

(sec), I_{ED} (mA), and T_a (°C) were correlated with the WO_3 thin-film thickness. The empirical formulas for the thickness of an as-deposited ($FT_{As\text{-}dep.}$, nm) and annealed ($FT_{An.}$, nm) WO_3 thin film are expressed as (3) and (4), respectively. The corresponding R^2 values are 0.946 and 0.843:

$$FT_{As\text{-}dep.} = 2.154t_{ED} + 35.125I_{ED} - 94.855, \quad (3)$$

$$FT_{An.} = 0.002t_{ED}^{2.5} + 20.838I_{ED} + 0.327T_a - 110.784. \quad (4)$$

Figures 8–10 show the transmittance, reflectivity, and absorptance of the WO_3-coated glass and ITO glass for various values of the process parameters. Table 2 lists the average transmittance, reflectivity, and absorptance of the WO_3-coated glass and ITO glass in VIS (400–760 nm) and NIR (760–2400 nm) region for various values of the process

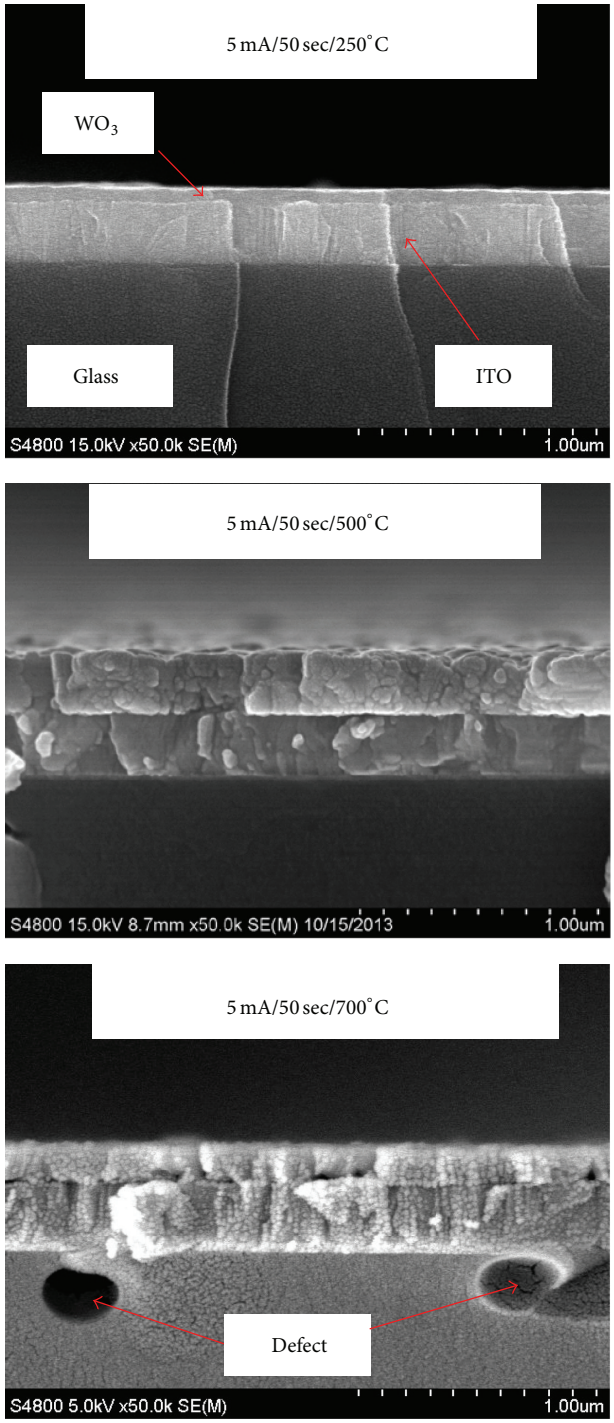

FIGURE 6: Cross-sectional FESEM image of the WO_3-coated glass.

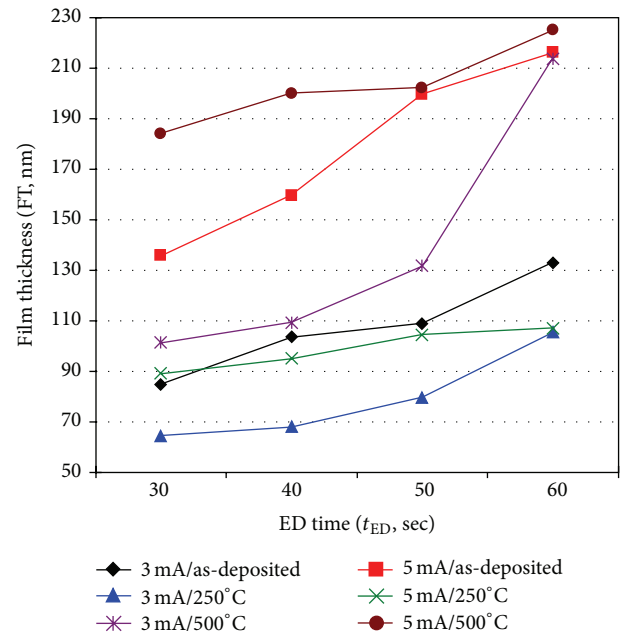

FIGURE 7: Variation of the WO_3 film thickness with various process parameters.

parameters. The transmittance, reflectivity, and absorptance of the WO_3-coated glass and ITO glass show similar trends at a given T_a. In Figures 8(a), 8(b), 9(a), and 9(b), and Table 2, the amorphous WO_3-coated glass and ITO glass ($T_a \leq 250^\circ C$) show high transmittance and low reflectivity in the VIS region. However, the transmittance decreases but the reflectivity increases as the wavelength increases in the NIR region. The experimental results for the transmittance of the amorphous WO_3-coated glass are in accordance with trends reported in the literature [3, 6].

The oscillations of amorphous WO_3-coated glass in the VIS region, which are associated with interferences between atomic layers, indicate the good quality of the WO_3 thin films [6]. The experimental results demonstrate that values of average transmittance of the amorphous WO_3-coated glass are 76.6% to 82.9% and 21.3% to 26.1% in the VIS and NIR regions, respectively; values of average reflectivity of the amorphous WO_3-coated glass are 11.4% to 17.8% and 43.4% to 49.8% in the VIS and NIR regions, respectively.

In Figures 8(c) and 9(c) and Table 2, the transmittance of the WO_3-coated glass annealed at 500°C in the VIS region is slightly lower than that of the amorphous WO_3-coated glass, but the transmittance and reflectivity of WO_3-coated glass ($T_a = 500^\circ C$) in the NIR region are, respectively, much higher and lower than those of the amorphous WO_3-coated glass, showing that anorthic WO_3 thin films have high transparency in NIR light [2]. In addition, the average reflectivity of the anorthic WO_3-coated glass is at least 17.8% lower than that of the amorphous WO_3-coated glass in the NIR region. The experimental results demonstrate that values of average transmittance of the anorthic WO_3-coated glass are 74.8% to 77.6% and 58.5% to 69.0% in the VIS and NIR regions, respectively; values of average reflectivity of the anorthic WO_3-coated glass are 16.1% to 18.8% and 9.7% to 25.6% in the VIS and NIR regions, respectively.

In Figure 10 and Table 2, the average absorptance of the amorphous WO_3-coated glass samples (as-deposited and annealed at 250°C) is less than 6.5% in the VIS region, and the absorptance gradually increases in oscillations at wavelengths in the NIR region. However, the average absorptance of the anorthic WO_3-coated glass ($T_a = 500^\circ C$) is less than

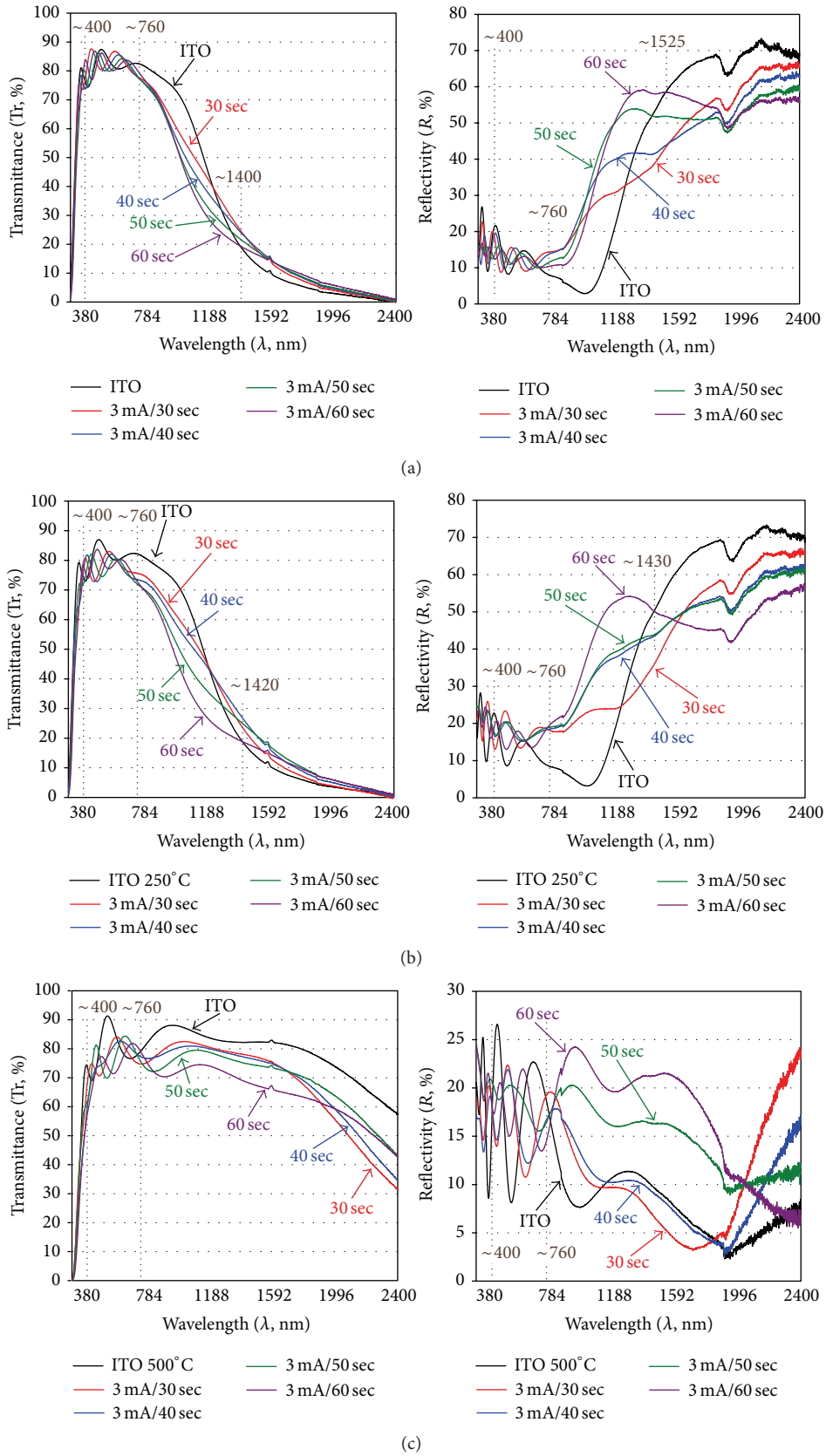

FIGURE 8: Transmittance and reflectivity of the WO_3-coated glass and ITO glass annealed at various T_a and at an I_{ED} of 3 mA: (a) as-deposited, (b) T_a = 250°C, and (c) T_a = 500°C.

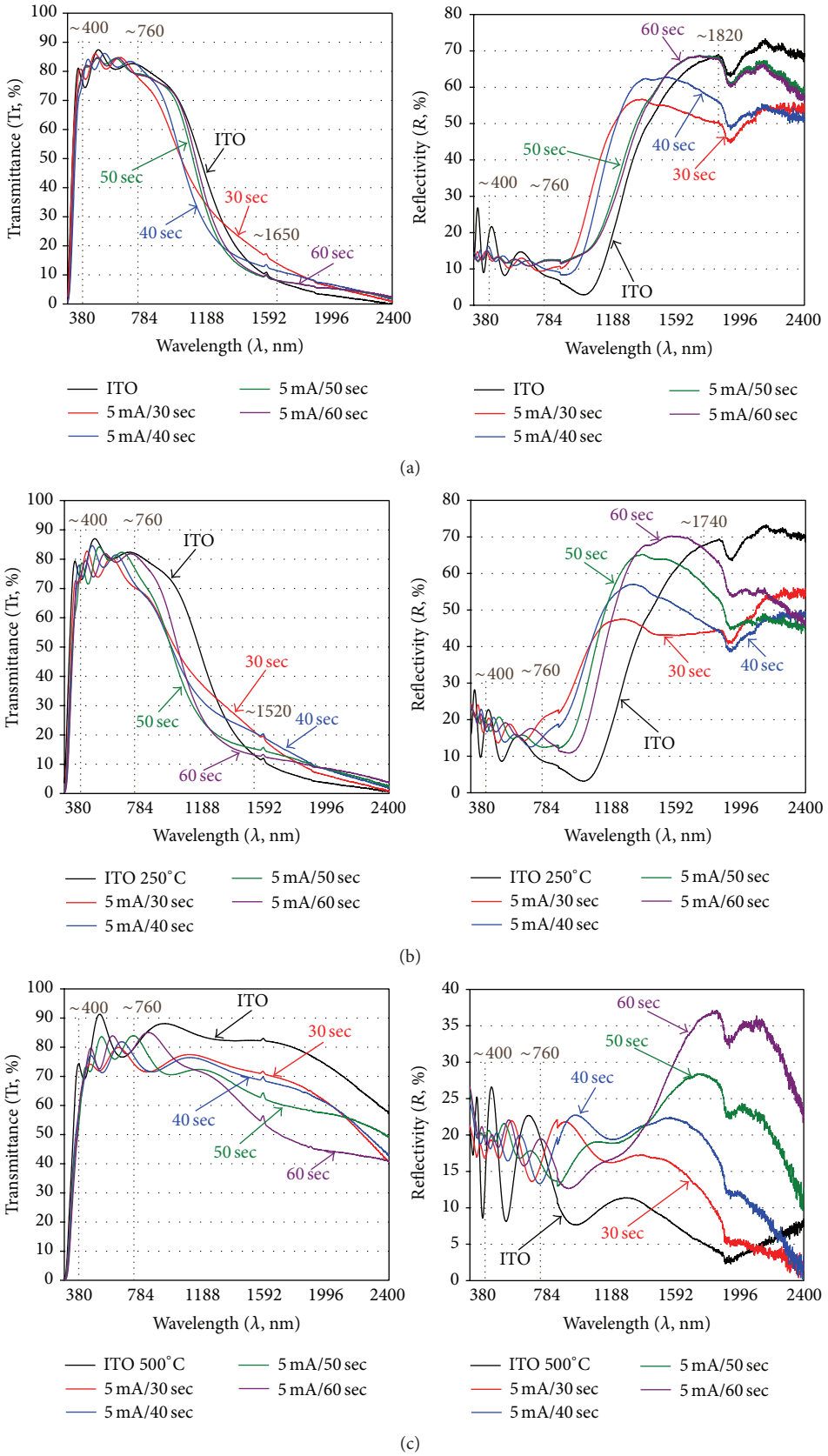

FIGURE 9: Transmittance and reflectivity of the WO_3-coated glass and ITO glass annealed at various T_a and at an I_{ED} of 5 mA: (a) as-deposited, (b) T_a = 250°C, and (c) T_a = 500°C.

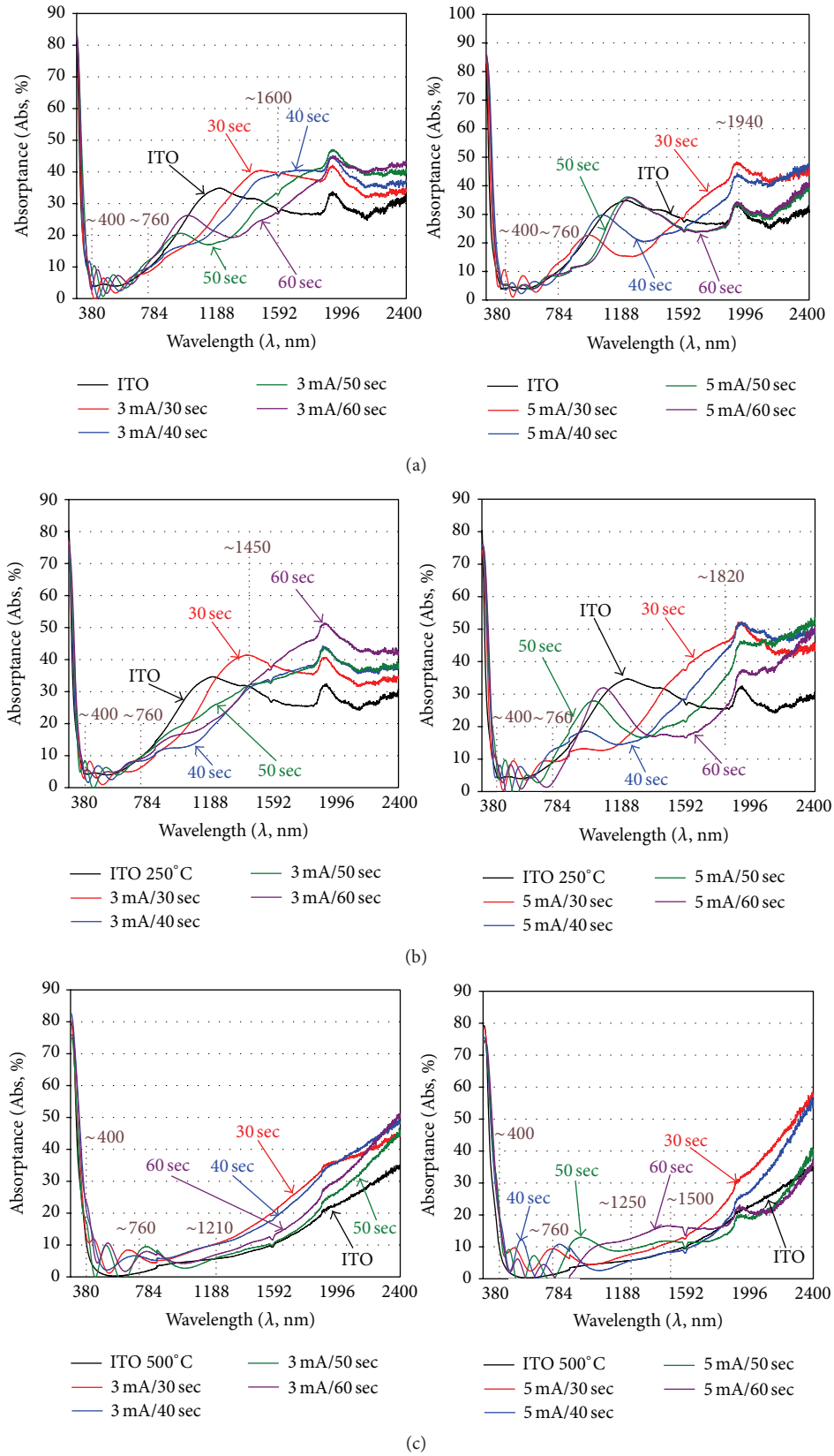

Figure 10: Absorptance of the WO_3-coated glass and ITO glass at various values of the process parameters: (a) as-deposited, (b) T_a = 250°C, and (c) T_a = 500°C.

Table 2: The average transmittance, reflectivity, and absorptance of the test samples.

Items	Annealing temperature	Region	I_{ED} (mA)	ITO	WO_3-coated glass							
				—	3				5			
			t_{ED} (sec)	—	30	40	50	60	30	40	50	60
Transmittance (%)	As-deposited	VIS		82.0	82.7	81.9	81.3	81.8	82.1	82.9	82.3	82.4
	250			81.5	77.9	77.2	77.0	78.1	76.6	78.5	79.5	79.2
	500			80.0	77.0	77.3	77.0	75.1	74.8	75.6	77.6	77.4
	As-deposited	NIR		25.5	24.9	24.1	22.9	22.5	24.5	23.1	23.9	24.7
	250			26.3	25.5	26.1	24.3	21.3	24.6	24.1	22.1	23.4
	500			78.4	67.2	68.1	69.0	64.5	66.8	66.1	63.9	58.5
Reflectivity (%)	As-deposited	VIS		12.6	12.3	12.7	12.4	12.0	11.4	12.0	12.1	12.0
	250			13.1	17.5	17.4	17.8	16.2	16.9	15.3	16.0	17.2
	500			18.4	16.2	16.1	18.3	17.6	17.7	17.5	18.6	18.8
	As-deposited	NIR		46.7	44.0	44.5	46.5	47.3	45.2	46.7	49.3	48.4
	250			46.6	43.4	45.4	45.2	45.8	43.4	44.5	47.3	49.8
	500			7.7	10.6	9.7	14.6	16.7	12.7	16.6	20.9	25.6
Absorptance (%)	As-deposited	VIS		5.4	4.9	5.4	6.4	6.2	6.5	5.2	5.6	5.6
	250			5.4	4.5	5.4	5.2	5.7	6.5	6.2	4.5	3.7
	500			1.5	6.8	6.6	4.7	7.2	7.6	6.9	3.7	3.8
	As-deposited	NIR		27.8	31.1	31.4	30.7	30.2	30.3	30.2	26.8	26.8
	250			27.1	31.1	28.6	30.5	32.8	32.0	31.4	30.6	26.8
	500			13.9	22.2	22.1	16.4	18.8	20.6	17.3	15.2	16.0

7.6% in the VIS region, and the absorptance increases in a relatively stable state with the wavelength in the NIR region, unlike the amorphous WO_3-coated glass. The experimental results demonstrate that values of average absorptance of the amorphous WO_3-coated glass are 3.7% to 6.5% and 26.8% to 32.8% in the VIS and NIR regions, respectively; values of average absorptance of the anorthic WO_3-coated glass are 3.7% to 7.6% and 15.2% to 22.2% in the VIS and NIR regions, respectively.

Although the transmittance, reflectivity, and absorptance of the WO_3-coated glass samples fabricated at various t_{ED} and I_{ED} with the same T_a show similar trends, they also display considerable differences at the same wavelength. The main reason for these differences is that the film thickness and surface roughness of the multilayered WO_3-coated glass samples varied with the I_{ED} and t_{ED}. The thickness of the thin film causes constructive or destructive interference of incident light, which affects both transmission and reflection spectrum. Moreover, surface roughness cause incident light scattering and thus affects both transmission and reflection spectrum.

5. Conclusions

WO_3 thin films were successfully prepared on ITO glass substrates through ED with various I_{ED}, t_{ED}, and T_a settings, and their characteristics were determined using appropriate instruments and test methods. The findings of this study are summarized as follows:

(1) To prepare WO_3-coated glass through ED, the optimal I_{ED} were 3–5 mA at various t_{ED} (30–60 s), and T_a less than 500°C can avoid damage and defects in the substrate (ITO glass).

(2) The WO_3 film thickness increased with t_{ED} and I_{ED}. However, T_a also notably affected the WO_3 film thickness.

(3) The as-deposited WO_3 thin films and WO_3 thin films annealed at 250°C were amorphous. By contrast, WO_3 thin films annealed at 500 and 700°C were in the anorthic phase.

(4) The amorphous WO_3-coated glass had high transmittance in VIS light and low transmittance in NIR light. However, the anorthic WO_3-coated glass had high transmittance in NIR light.

(5) Multiple regression and ED process parameters were used to derive an empirical formula for determining the thickness of WO_3 thin films.

(6) The amorphous WO_3 thin films are typically used in an electrochromic device. In addition, the amorphous and uneven crystalline WO_3 thin films can also be applied to the fields of spectral selection, gas sensors, lithium-ion battery electrodes, antiwear coating, and catalysis according to its characteristics (e.g., uneven surface of WO_3 thin film may benefit reaction with external substances).

Competing Interests

The authors declare that there is no conflict of interests regarding the publication of this paper.

Acknowledgments

The authors would like to thank National Science Council of the Republic of China, for their financial support to this research under Contract no. NSC 102-2221-E-003-006-.

References

[1] M. Deepa, A. K. Srivastava, T. K. Saxena, and S. A. Agnihotry, "Annealing induced microstructural evolution of electrodeposited electrochromic tungsten oxide films," *Applied Surface Science*, vol. 252, no. 5, pp. 1568–1580, 2005.

[2] M. Deepa, A. K. Srivastava, S. Lauterbach, Govind, S. M. Shivaprasad, and K. N. Sood, "Electro-optical response of tungsten oxide thin film nanostructures processed by a template-assisted electrodeposition route," *Acta Materialia*, vol. 55, no. 18, pp. 6095–6107, 2007.

[3] M. Deepa, A. K. Srivastava, S. N. Sharma, Govind, and S. M. Shivaprasad, "Microstructural and electrochromic properties of tungsten oxide thin films produced by surfactant mediated electrodeposition," *Applied Surface Science*, vol. 254, no. 8, pp. 2342–2352, 2008.

[4] K. A. Gesheva, T. M. Ivanova, and G. Bodurov, "Transition metal oxide films: technology and Smart Windows electrochromic device performance," *Progress in Organic Coatings*, vol. 74, no. 4, pp. 635–639, 2012.

[5] C.-K. Wang, C.-K. Lin, C.-L. Wu, S. Brahma, S.-C. Wang, and J.-L. Huang, "Characterization of electrochromic tungsten oxide film from electrochemical anodized RF-sputtered tungsten films," *Ceramics International*, vol. 39, no. 4, pp. 4293–4298, 2013.

[6] Ö. Tuna, A. Sezgin, R. Budakoğlu, S. Türküz, and H. Parlar, "Electrochromic properties of tungsten trioxide (WO_3) layers grown on ITO/glass substrates by magnetron sputtering," *Vacuum B*, vol. 120, pp. 28–31, 2015.

[7] G. Gorgolis and D. Karamanis, "Solar energy materials for glazing technologies," *Solar Energy Materials and Solar Cells*, vol. 144, pp. 559–578, 2016.

[8] J. Georgieva, E. Valova, S. Armyanov, N. Philippidis, I. Poulios, and S. Sotiropoulos, "Bi-component semiconductor oxide photoanodes for the photoelectrocatalytic oxidation of organic solutes and vapours: a short review with emphasis to TiO_2–WO_3 photoanodes," *Journal of Hazardous Materials*, vol. 211-212, pp. 30–46, 2012.

[9] S. S. Thind, K. Rozic, F. Amano, and A. Chen, "Fabrication and photoelectrochemical study of WO_3-based bifunctional electrodes for environmental applications," *Applied Catalysis B: Environmental*, vol. 176-177, pp. 464–471, 2015.

[10] S. Ghosh, S. S. Acharyya, R. Singh, P. Gupta, and R. Bal, "Fabrication of Ag/WO_3 nanobars for Baeyer-Villiger oxidation using hydrogen peroxide," *Catalysis Communications*, vol. 72, pp. 33–37, 2015.

[11] X. Wang, L. Pang, X. Hu, and N. Han, "Fabrication of ion doped WO_3 photocatalysts through bulk and surface doping," *Journal of Environmental Sciences*, vol. 35, pp. 76–82, 2015.

[12] S. Ashraf, C. S. Blackman, R. G. Palgrave, and I. P. Parkin, "Aerosol-assisted chemical vapour deposition of WO_3 thin films using polyoxometallate precursors and their gas sensing properties," *Journal of Materials Chemistry*, vol. 17, no. 11, pp. 1063–1070, 2007.

[13] K. Wetchakun, T. Samerjai, N. Tamaekong et al., "Semiconducting metal oxides as sensors for environmentally hazardous gases," *Sensors and Actuators B: Chemical*, vol. 160, no. 1, pp. 580–591, 2011.

[14] H. Y. Li, Z. X. Cai, J. C. Ding, and X. Guo, "Gigantically enhanced NO sensing properties of WO_3/SnO_2 double layer sensors with Pd decoration," *Sensors and Actuators B: Chemical*, vol. 220, pp. 398–405, 2015.

[15] J. Ollitrault, N. Martin, J.-Y. Rauch, J.-B. Sanchez, and F. Berger, "Improvement of ozone detection with GLAD WO_3 films," *Materials Letters*, vol. 155, pp. 1–3, 2015.

[16] F. Li, C. Li, L. Zhu et al., "Enhanced toluene sensing performance of gold-functionalized $WO_3 \cdot H_2O$ nanosheets," *Sensors and Actuators B: Chemical*, vol. 223, pp. 761–767, 2016.

[17] W.-J. Li and Z.-W. Fu, "Nanostructured WO_3 thin film as a new anode material for lithium-ion batteries," *Applied Surface Science*, vol. 256, no. 8, pp. 2447–2452, 2010.

[18] L. Gao, X. Wang, Z. Xie et al., "High performance energy-storage devices based on WO_3 nanowire arrays/carbon cloth integrated electrodes," *Journal of Materials Chemistry A*, vol. 1, no. 24, pp. 7167–7173, 2013.

[19] L. Gao, F. Qu, and X. Wu, "Hierarchical WO_3@SnO_2 core–shell nanowire arrays on carbon cloth: a new class of anode for high-performance lithium-ion batteries," *Journal of Materials Chemistry A*, vol. 2, no. 20, pp. 7367–7372, 2014.

[20] S. K. Park, H. J. Lee, M. H. Lee, and H. S. Park, "Hierarchically structured reduced graphene oxide/WO_3 frameworks for an application into lithium ion battery anodes," *Chemical Engineering Journal*, vol. 281, pp. 724–729, 2015.

[21] O. D. Greenwood, S. C. Moulzolf, P. J. Blau, and R. J. Lad, "The influence of microstructure on tribological properties of WO_3 thin films," *Wear*, vol. 232, no. 1, pp. 84–90, 1999.

[22] P. Harlin, P. Carlsson, U. Bexell, and M. Olsson, "Influence of surface roughness of PVD coatings on tribological performance in sliding contacts," *Surface and Coatings Technology*, vol. 201, no. 7, pp. 4253–4259, 2006.

[23] V. Totolin, M. Rodríguez Ripoll, M. Jech, and B. Podgornik, "Enhanced tribological performance of tungsten carbide functionalized surfaces via in-situ formation of low-friction tribofilms," *Tribology International*, vol. 94, pp. 269–278, 2016.

[24] S. Ashraf, C. S. Blackman, S. C. Naisbitt, and I. P. Parkin, "The gas-sensing properties of WO3-x thin films deposited via the atmospheric pressure chemical vapour deposition (APCVD) of WCl6 with ethanol," *Measurement Science and Technology*, vol. 19, no. 2, Article ID 025203, 2008.

[25] E. A. Meulenkamp, "Mechanism of WO_3 electrodeposition from peroxy-tungstate solution," *Journal of the Electrochemical Society*, vol. 144, no. 5, pp. 1664–1671, 1997.

[26] Y. O. Kim, S. Yu, K. Ahn, S. K. Lee, and S. H. Kang, "Enhancing the photoresponse of electrodeposited WO_3 film: structure and thickness effect," *Journal of Electroanalytical Chemistry*, vol. 752, pp. 25–32, 2015.

[27] A. J. More, R. S. Patil, D. S. Dalavi et al., "Electrodeposition of nano-granular tungsten oxide thin films for smart window application," *Materials Letters*, vol. 134, pp. 298–301, 2014.

[28] K. P. S. S. Hembram, R. Thomas, and G. M. Rao, "Microstructural evolution of tungsten oxide thin films," *Applied Surface Science*, vol. 256, no. 2, pp. 419–422, 2009.

[29] Y. Fang, W. C. Lee, G. E. Canciani et al., "Thickness control in electrophoretic deposition of WO_3 nanofiber thin films for solar water splitting," *Materials Science and Engineering B: Solid-State Materials for Advanced Technology*, vol. 202, Article ID 13793, pp. 39–45, 2015.